ACS OMEGA

http://pubs.acs.org/journal/acsodf

Article

Corrosion Mitigation Performance of N80 Steel in 5% Sulfamic Acid Medium by Applying Novel Tetrahydro-1,2,4-triazines Including Triazene Moieties: Electrochemical and Theoretical Approaches

Hany M. Abd El-Lateef,* Kamal Shalabi, Anas M. Arab, and Yasser M. Abdallah*

Cite This: *ACS Omega* 2022, 7, 23380−23392

Read Online

ACCESS | Metrics & More | Article Recommendations

ABSTRACT: We observed our newly developed tetrahydro-1,2,4-triazines, including triazene moieties (**THTA**), namely, 6-((1E)-1-((2E)-(4-(((Z)-1-(2,4-diphenyl-2,3,4,5-tetrahydro-1,2,4-triazin-5-yl) ethylidene) triaz-1-en-1-yl)piperazin-1-yl) triaz-2-en-1-ylidene) ethyl)-2,4-diphenyl-2,3,4,5-tetrahydro-1,2,4-triazine (**THTA-I**), and 1-((E)-((E)-1-(2,4-diphenyl-2,3,4,5-tetrahydro-1,2,4-triazin-6-yl) ethylidene) triaz-1-en-1-yl) naphthalen-2-ol (**THTA-II**), as effective inhibitors for the corrosion protection of N80 carbon steel metal in 5% sulfamic acid as the corrosive medium via electrochemical approaches such as potentiodynamic polarization and electrochemical impedance spectroscopy. Furthermore, the tested steel exterior was monitored using X-ray photoelectron spectroscopy after the treatment with the investigated components to verify the establishment of the adsorbed shielding film. The investigated compounds acted as mixed-type inhibitors, as shown by Tafel diagrams. The compounds considered obey the Langmuir adsorption isotherm, and their adsorption on the steel surface was chemisorption. When the tested inhibitors were added, the double-layer capacitances, which can be determined by the adsorption of the tested inhibitors on N80 steel specimens, decreased compared with that of the blank solution. At 10^{-4} M, the inhibitory efficacy of **THTA-I** and **THTA-II** achieved maximum values of 88.5 and 86.5%, respectively. Density-functional theory computations and Monte-Carlo simulation were applied to determine the adsorption attributes and inhibition mechanism through the studied components. Furthermore, the investigated inhibitors were considered to adsorb on the Fe (1 1 0) surface. The adsorption energy was then measured on steel specimens.

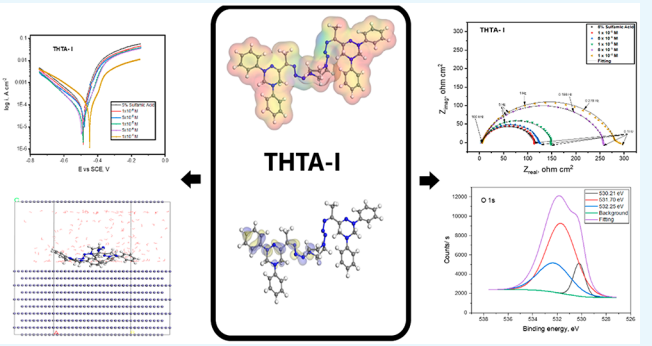

1. INTRODUCTION

Corrosion progression plays a crucial role in the economy and preservation of alloys and metals. N80 carbon steel is extensively operated as a structural material in industries, therapeutic applications, propulsion applications, petroleum applications, and food manufacturing. The corrosion of carbon steel petroleum lines is a complex process that leads to considerable problems owing to localized corrosion because certain solutions (i.e., media) are aggressive. Corrosion can be mitigated by the addition of inhibitors in smaller amounts. Organic compounds including heteroatoms like S, N, and O are the most effective inhibitors.[1−5] As per the present data, organic components with functional groups such as −OH, $-NH_2$, $-OCH_3$, −COOH, and $-SO_3H$ as well as benzene moieties containing heteroatoms may be effective inhibitors because they can react with the studied metal or alloy to form a protective film on the inspected exterior.[6−9]

Although their corrosion properties are weaker than those of H_3PO_4, HCl, and H_2SO_4, the aquatic solutions of sulfamic acid have been examined as a forceful acid; their dissolved maximal industrial accumulation is determined by creating soluble components through sulfamic acid.[10] To prevent the corrosion of investigated metals, researchers should add organic inhibitors to the acid purification of pipes, cylinders, and apparatus composed of several types of steels.[11,12]

Various amino acids,[13] tetra-pyridinium components,[14] azo dye-particles,[15] aquatic root extract of *Salvadora persica*,[16] monomeric and Gemini surfactants,[17] and cationic surfactants,[18] were reported as corrosion inhibitors for carbon steel in corrosive sulfamic acid environments. Consequently, triazine derivatives indicate a great assurance as inhibitors for biological and pharmaceutical applications, for example, antibacterial,[19] analgesic,[20] antiviral,[21] antimalarial,[22] antitumor, and cytotoxic

Received: March 18, 2022
Accepted: June 14, 2022
Published: June 24, 2022

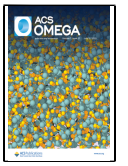

Table 1. Molecular Weight and Chemical Composition of Inhibitors under Investigation

inhibitor	name	structure	molecular weight and molecular composition
THTA- I	6-((1E)-1-((2E)-(4-(((Z)-1-(2,4-diphenyl-2,3,4,5-tetrahydro-1,2,4-triazin-5-yl)ethylidene)triaz-1-en-1-yl)piperazin-1-yl)triaz-2-en-1-ylidene)ethyl)-2,4-diphenyl-2,3,4,5-tetrahydro-1,2,4-triazine	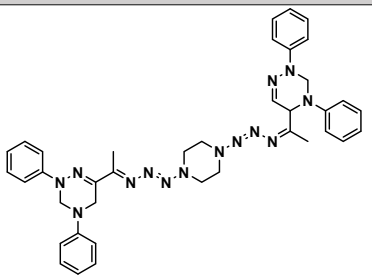	**chemical formula:** $C_{38}H_{42}N_{14}$ **molecular weight:** 694.85 **elemental analysis:** C, 65.69; H, 6.09; N, 28.22
THTA- II	1-((E)-((E)-1-(2,4-diphenyl-2,3,4,5-tetrahydro-1,2,4-triazin-6-yl)ethylidene)triaz-1-en-1-yl)naphthalen-2-ol	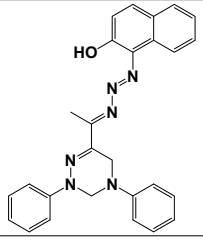	**chemical formula:** $C_{27}H_{24}N_6O$ **molecular weight:** 448.53 **elemental analysis:** C, 72.30; H, 5.39; N, 18.74; O, 3.57

activities.[23] Organic compounds, including thiazole moieties, have previously been explained as biologically active operatives, such as vitamin B1 (thiamine), thus improving the nervous system function,[24] and multiple general thiazole-containing antibiotics.[25]

Quantum chemical concepts have been extensively used to understand corrosion mechanisms and clarify experimental data and interpret chemical ambiguity. The use of such concepts is an appropriate technique for examining the corrosion reaction mechanisms of organic inhibitory compounds with the examined surface.

This paper aimed to examine the influence of tetrahydro-1,2,4-triazines including triazene derivatives, on the corrosion prohibition of N80 steel in 5% sulfamic acid solutions through potentiodynamic polarization (**PP**) and electrochemical impedance spectroscopy (**EIS**) proportions. Furthermore, X-ray photoelectron spectroscopy (**XPS**) was used to scan the surface morphology to demonstrate the deposited protective coating on the N80 steel. To demonstrate energetic cores and prohibition mechanisms of corrosion processes for the investigated **THTA** compounds, we applied quantum chemical calculations (**DFT**) using Fukui indices, Mulliken atomic charges, molecular electrostatic potential (**MEP**) mapping, and Monte-Carlo (**MC**) simulations.

2. MATERIALS AND METHODS

2.1. Materials and Reagents. In this study, an N80 carbon steel sample [constitution (weight percent): C (0.31%), S (0.008%), P (0.01%), Si (0.19%), Mn (0.92%), Cr (0.20%), and the remainder comprised Fe] with an effective surface of ≈1 cm^2 was utilized as the working electrode and scraped using emery papers of various grades (up to 1000 grade), degreased with propanone, rinsed with doubly distilled water, and desiccated with faint tissues. Trials were conducted in 5% sulfamic acid solution in the absence and presence of various portions of the investigated tetrahydro-1,2,4-triazines incorporating triazene derivations outlined in previous work[26] (Table 1). For each experiment, the concentrations of the analyzed components ordered from 1×10^{-6} M to 1×10^{-4} M; a freshly discarded solution was used.

2.2. Electrochemical Measurements. An N80 carbon steel sample was utilized as the working electrode, which was attached to the epoxy resin of polytetrafluoroethylene, a saturated calomel electrode (SCE) as the auxiliary electrode, and a Pt wire as the assembly conductor. To reduce the IR drop, we linked the auxiliary conductor to a Luggin capillary tube, and the head of the capillary was located near to the working electrode. The reaction chamber was released in the atmosphere; all tests were conducted at 25 ± 1 °C. The potential standards were calibrated vs SCE. Before every measurement, the N80 carbon steel surface was scratched with various emery papers, cleaned with a basic solution (15 g Na_2CO_3 + 15 g Na_3PO_4 by liter),[27] rinsed with deionized water, and then wiped.

The electrode potential was adjusted between −0.8 and 0.2 V versus SCE using a scan rate of 1 mVs^{-1} at an open circuit potential to achieve the PP results. The Stern Geary process[28,29] was used to determine the corrosion current by calculating the cathodic and anodic Tafel figures of charge transfer restrained corrosion to a spot that obtains (log i_{corr}) and the equivalent corrosion potential (E_{corr}) for 5% sulfamic acid medium, and the concentrations of the studied triazene inhibitors (**THTA**). Subsequently, i_{corr} was used to assess the prohibition capability and surface coverage (θ) using the following equation:

$$\%\eta = \theta \times 100 = \left(1 - \frac{i_{corr(inh)}}{i_{corr(free)}}\right) \times 100 \quad (1)$$

wherever $i_{corr(free)}$ and $i_{corr(inh)}$ are the corrosion current densities in the presence and absence of the examined **THTA** components, respectively.

EIS investigations were executed in the frequency range of 100,000 to 0.1 Hz, thus resulting in a peak-to-peak voltage of 10 mV through AC signals at open circuit potential.

Impedance experiments were conducted, and the result for the constructed circuit was explained. The polarization resistance R_p and double-layer capacity of C_{dl}, which were determined, were the intended variables concluded with the examination of Nyquist semicircles as follows:

https://doi.org/10.1021/acsomega.2c01629
ACS Omega 2022, 7, 23380−23392

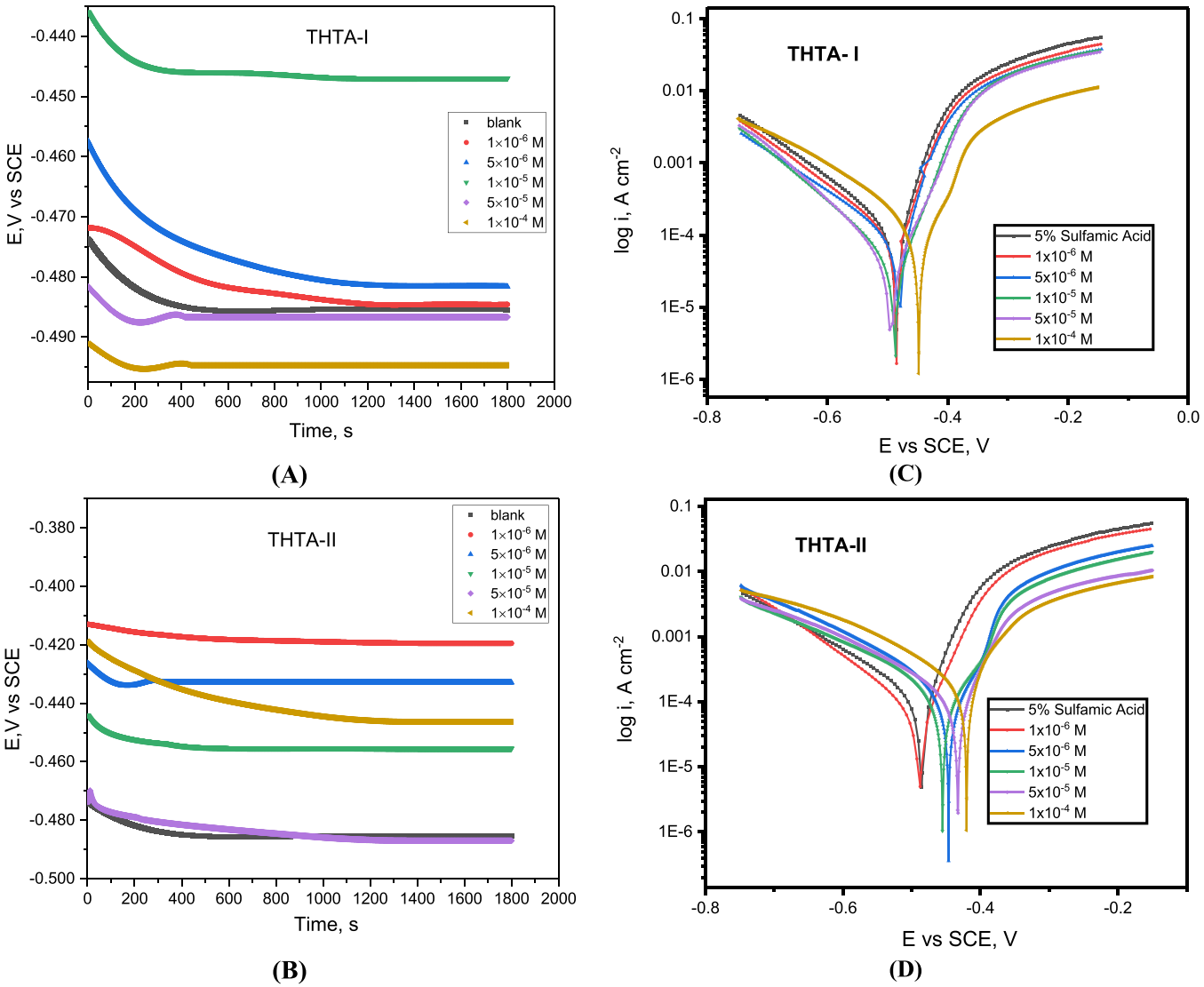

Figure 1. E_{ocp} vs time measurements (A,B) and Tafel diagrams (C,D) for N80 carbon steel corrosion in corrosive medium containing 5% sulfamic acid in the absence and presence of different doses of **THTA-I** (A,C) and **THTA-II** (B,D) at 25 ± 1 °C

$$C_{dl} = \frac{1}{(2\pi f_{max} R_p)} \quad (2)$$

wherever f_{max} is the angular frequency when the imaginary part of the impedance expands the most. The following equation was used to compute the impedance method's prohibition capability and surface coverage (θ):

$$\%\eta = \theta \times 100 = \left(1 - \left[\frac{R_p^{\circ}}{R_p}\right]\right) \times 100 \quad (3)$$

The electrode potential was permitted to stabilize for 30 min prior to each measurement, which was performed at 25 °C. A Gamry Reference 3000 was used to perform electrochemical measurements using a potentiostat/galvanostat/ZRA with Gamry Framework version 6.33 software set up on a PC for leading and result registration. Echem Analyst version 6.33 software was used for statistic planning and analysis. For the agreement and guarantee of investigations, all tests were conducted on a regular basis in a similar state. Each electrochemical test was repeated three times to emphasize data duplicability.

2.3. Surface Investigation by XPS. High-resolution XPS examination was carried out through K-ALPHA (Thermo Fisher Scientific, USA) with monochromatic X-ray Al K-alpha radiation to unrestrained and restrained N80 specimens in 5% sulfamic acid using 1 × 10^{-4} M 6-((1E)-1-((2E)-(4-(((Z)-1-(2,4-diphenyl-2,3,4,5-tetrahydro-1,2,4-triazin-5-yl) ethylidene) triaz-1-en-1-yl)piperazin-1-yl) triaz-2-en-1-ylidene) ethyl)-2,4-diphenyl-2,3,4,5-tetrahydro-1,2,4-triazine (**THTA-I**) for 24 h at 25 ± 1 °C.

2.4. Density-Functional Theory (DFT) Calculations and MC Simulations. To consider the corrosion mechanism, the association within theoretical characteristics, and experimental results, the inhibition efficiencies were efficiently analyzed. Computerized analyses were completed using Accelrys Materials Studio 7.0[30] including the DMol3 module for DFT calculations and the adsorption locator module for MC simulations. The configurations of triazine components were optimized in DFT calculations utilizing the GGA/BLYP functional with set DNP foundation and COSMO solvation controls.[30] The best proper adsorption preparations of the

https://doi.org/10.1021/acsomega.2c01629
ACS Omega 2022, 7, 23380−23392

Table 2. Tafel Polarization Parameters for Corrosion of N80 Carbon Steel in 5% Sulfamic Acid Solution with and without Different THTA Compound Concentrations at 25 ± 1 °C

inhibitor	conc., (M)	$-E_{corr}$ mV (vs SCE)	i_{corr}, μAcm^{-2}	β_a, mV dec^{-1}	β_c, mV dec^{-1}	corrosion rate mpy	Θ	IE %
5% sulfamic acid (BLANK)		486	257.0 ± 13.7	170.1	217.3	117.6		
THTA-I	1×10^{-6}	485	92.1 ± 4.9	119.1	205.4	80.43	0.642	64.2
	5×10^{-6}	482	88.6 ± 4.5	126.1	220.4	69.09	0.655	65.5
	1×10^{-5}	448	73.9 ± 3.5	85.8	168.9	59.65	0.712	71.2
	5×10^{-5}	488	46.8 ± 2.2	139.7	187.8	42.87	0.818	81.8
	1×10^{-4}	495	39.2 ± 1.9	119.5	167	38.03	0.847	84.7
THTA-II	1×10^{-6}	420	98.5 ± 5.2	56	181.7	84.28	0.617	61.7
	5×10^{-6}	433	90.0 ± 4.7	64.1	179.8	55.19	0.650	65.0
	1×10^{-5}	455	75.0 ± 4.0	74.3	147.2	47.74	0.708	70.8
	5×10^{-5}	489	49.7 ± 2.6	92.1	228.5	43.76	0.807	80.7
	1×10^{-4}	446	42.4 ± 2.3	56.5	117.4	39.32	0.835	83.5

triazine derivative inhibitors on the Fe (1 1 0) surface were demonstrated using the adsorption locator module in MC simulations to estimate the prohibition tendency of the tested inhibitors.[31] The **THTA** component adsorption with water particles and examined surface of Fe (1 1 0) was obtained using a simulating box (32.27 × 32.27 × 50.18 Å^3) and the assigned COMPASS force field.[32] Moreover, all the theoretical analyses' entries, results, and computations were reflected in our recently published publications.[30,31]

3. RESULTS AND DISCUSSION

3.1. E_{ocp} vs Time and PP Studies. *3.1.1. Effect of Triazene Component Concentrations.* Figure 1,A and B reveals the change of E_{ocp} vs time for inhibited and uninhibited N80 steel in 5% sulfamic acid solutions during 30 min exposure time. As shown in Figure 1,BA, the N80 steel in uninhibited and inhibited solutions reaches a stable state after ≈ 400 s immersion, and the values of E_{ocp} exhibit a small adjustment (< 0.001 V vs SCE). The primary value of the blank specimen was −0.474 V vs SCE, and it reached steady state near −0.485 V vs SCE. For inhibited specimens with triazene derivatives, the values of E_{ocp} shifted less than 85 mV compared to the uninhibited specimen for the period of the immersion indicating that triazene derivatives serve as mixed-type inhibitors. The values of E_{ocp} slightly reduced with the immersion period up to ≈400 s. The disturbed period could be ascribed to desorption and adsorption of the triazene derivatives at the interface of N80 steel/sulfamic acid. After the exposure period ≈400 s, the E_{ocp} values predisposed to steady, demonstrating that the adsorption and desorption of triazene derivatives had affected a stable equilibrium.

The corrosion performance of the N80 steel in 5% sulfamic acid solutions using the triazene derivatives as corrosion inhibitors was investigated using the PP approach at 25 ± 1 °C. Cathodic−anodic curves were determined with and without the examined inhibitors, as shown in Figure 1C,D for **THTA-I** and **THTA-II**, respectively. The corrosion potential (E_{corr}), corrosion current density (i_{corr}) acquired utilize polarization plots by extrapolation, anodic and cathodic Tafel slopes (β_a and β_c), the exposure surface (θ), and prohibition efficiency (%IE) are recorded in Table 2 and acquired by eq 1.

With the increase in the inhibitor concentrations of analyzed inhibitors, Tafel polarization plots demonstrated that the investigated compounds[33] displaced either anodic or cathodic curves to small current densities, indicating that **THTA** molecules are mixed-type inhibitors. Moreover, the corrosion current density was reduced from 275 μA cm^{-2} to 39.2 and 42.4 μA cm^{-2} in the presence of 1.0 × 10^{-4} M **THTA-I** and **THTA-II** inhibitors, respectively.

Table 2 shows that the rising of the tested inhibitor concentrations from 1 × 10^{-6} M to 1 × 10^{-4} M enhanced the inhibition capacity percentage (% IE). The corrosion potentials (E_{corr}) were slightly changed by the addition of **THTA** components, indicating that these molecules were mixed-type inhibitors. The anodic and cathodic Tafel slope (β_a and β_c) values were altered by the increase concentrations, indicating that **THTA** compounds affected the dissolution mechanism and evolution of hydrogen reactions.[34,35] Table 2 shows that the inhibitory power of **THTA-I** was greater than that of **THTA-II** at various dosages.

3.1.2. Adsorption Isotherm. Based on the adsorption mechanism of **THTA** compounds on N80 specimens, all examined **THTA** components limited the corrosion approach. Equation 4 shows the adsorption of the **THTA** compound at the metal/solution interface, which occurred when water molecules were replaced by **THTA** compounds.[36]

$$\mathrm{THTA}_{(sol)} + x\mathrm{H_2O}_{(ads)} \rightarrow \mathrm{THTA}_{(ads)} + x\mathrm{H_2O}_{(sol)} \quad (4)$$

where **THTA** $_{(sol)}$ and **THTA** $_{(ads)}$ denote the **THTA** components in the solution and adsorbed on the N80 carbon steel exterior, correspondingly, and x is the number of water molecules that have been replaced by **THTA** particles.

The following formula can be used to calculate the surface exposure (θ) by **THTA** particles:

$$\theta = \left[1 - \frac{i_{corr}}{i^{o}_{corr}}\right] \quad (5)$$

wherever θ is the different adsorption isotherm classes obtained by determining the best adsorption isotherm type. We also examined these investigated inhibitors by different isotherms as the Flory−Huggins isotherm (R^2 = 0.228, for **THTA- I** and R^2 = 0.224 for **THTA-II**), Temkin (R^2 = 0.899, for **THTA-I** and R^2 = 0.889 for **THTA-II**), and Frumkin (R^2 = 0.817, for **THTA-I** and R^2 = 0.800 for **THTA-2**). All the **THTA** inhibitors fitted the Langmuir isotherm type (R^2 = 0.999, for **THTA-I** and R^2 = 0.999 for **THTA-II**). eq 6, which provides a straight line with a coefficient constant (R^2) of singularity at 25 ± 1 °C and slope equal to unity, explains the relationship between C and C/θ (Figure 2).

$$\frac{C}{\theta} = \frac{1}{K_{ads}} + C \quad (6)$$

https://doi.org/10.1021/acsomega.2c01629
ACS Omega 2022, 7, 23380−23392

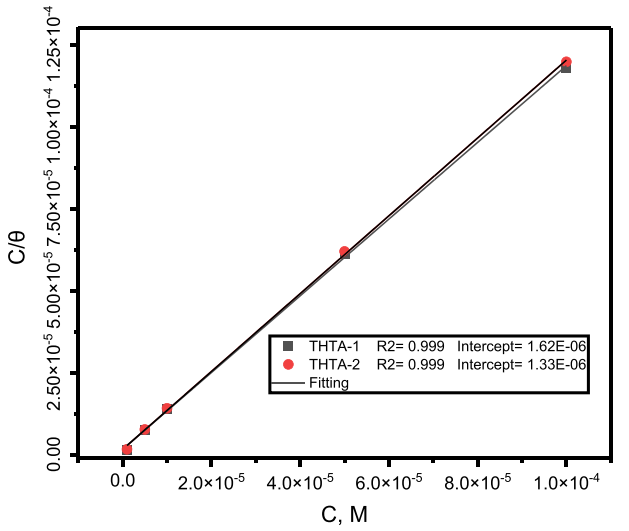

Figure 2. Langmuir adsorption isotherm fitting for corrosion data for of N80 steel in 5% sulfamic acid within different portions of the investigated **THTA** compounds at 25 ± 1 °C.

wherever C stands for the inhibitor's concentrations and K_{ads} refers to the adsorption process equilibrium constant, which is linked to the standard free energy of adsorption method (ΔG^0_{ads}) and can be derived using eq 7:[37]

$$K_{ads} = \frac{1}{55.5}\exp\left(\frac{-\Delta G^{\circ}_{ads}}{RT}\right) \quad (7)$$

whenever 55.5 is the apparent concentration of water solution expressed in (mol/L), (T) is the absolute temperature expressed in K (°C + 273.15), and (R) is the universal gas constant. The values of (θ) obtained from the polarization method were compared with a chart to determine the best adsorption isotherm, indicating that the adsorption of the tested **THTA** compounds on the N80 surface (Figure 2) followed the Langmuir adsorption isotherm.[38,39]

Using eq 7, the standard free energy of adsorption (ΔG^0_{ads}) for **THTA-I** was −42.9 kJ mol^{-1} (K_{ads} = 6.17 × 10^5 L mol^{-1}) and that for **THTA-II** was −43.5 kJ mol^{-1} (K_{ads} = 7.53 × 10^5 L mol^{-1}). Charge transfer with the evaluated **THTA** compounds against the steel surface to create a coordinate bond (chemisorption adsorption)[40] and a high negative criterion of (ΔG^0_{ads}) (i.e., −40 kJ mol^{-1} or above) demonstrated that the tested **THTA** compounds were spontaneously adsorbed on the steel surface.[41] Moreover, the creation of coordinate bonds with active locations of the investigated **THTA** (N atoms and π-orbital of double bonds) with vacant d-orbitals of the steel surface maintained the ΔG^0_{ads} values of **THTA** molecules nearly stable for the studied steel surface.

3.2. EIS Measurements. The Nyquist and Bode graphs for N80 carbon steel in 5% sulfamic acid corrosive medium with and without various dosages of **THTA** particles are demonstrated in Figure 3A,B and Figure 4A,B. The semicircle radius is used to express charge transfer resistance; hence the values of R_{ct} for N80 steel in the corrosive medium of 5% sulfamic acid were low compared to when **THTA** inhibitors (1 × 10^{-4} M) were added (i.e., the radius increased).

Figure 3A,B and Figure 4A,B demonstrate an impaired arch figure, an impedance smoothing within the center below the real axle, and depressed loops expanding significantly with captivation time, which is a normal action for the N80 steel

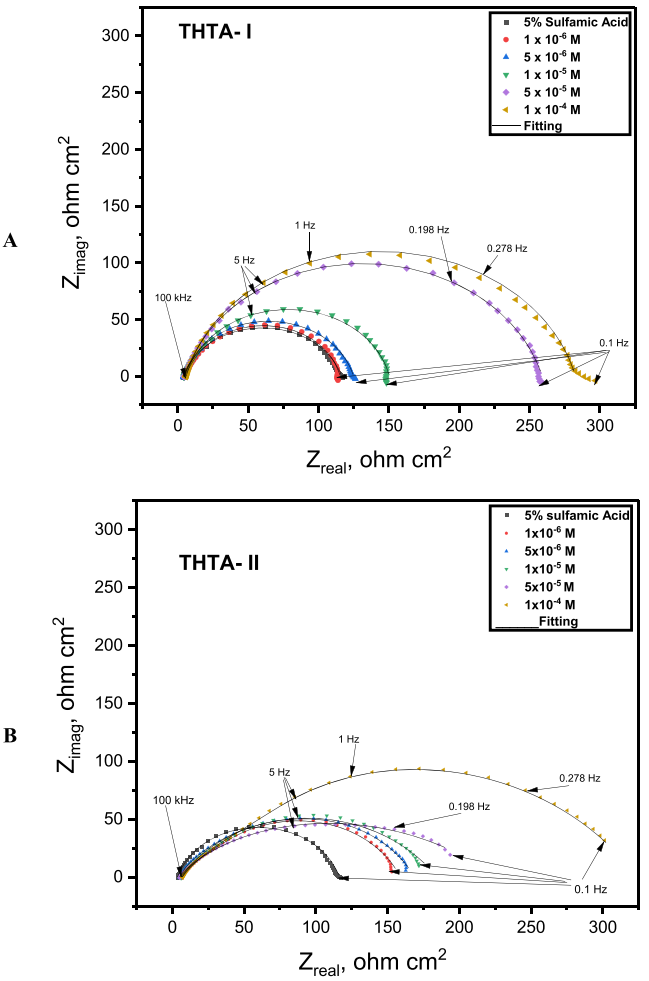

Figure 3. Nyquist diagrams for the corrosion of N80 CS in 5% sulfamic acid medium including different portions of **THTA** compounds (A) **THTA-I** and (B) **THTA-II** at 25 ± 1 °C.

electrode that displayed frequency dispersion for the impedance results,[42,43] which are confirmed with abnormality and extra inhomogeneity of the N80 surface.[44,45]

For inhibited solutions, two-time constants appeared in the EIS plots at small frequencies (Nyquist and Bode diagrams), whereas the blank solution demonstrated the configuration of a prohibitive barrier on the N80 carbon steel surface.

To examine the aforementioned achieved impedance calculations, we proposed the corresponding electric circuit structure in Figure 5a,b, wherever R_s is the solution resistance, R_f is the examined compound film resistance, CPE_f is the constant-phase element of the tested component film, CPE_{dl} is the constant-phase element of the double layer, and R_{ct} is the charge transfer resistance.

The protection efficacy for the corrosion of N80 steel (%IE) in the corrosive solution of 5% sulfamic acid was received with the polarization resistance R_p by the following formulas:[46]

$$R_p = R_f + R_{ct} \quad (8)$$

$$\%IE = \theta \times 100 = \left(1 - \left[\frac{R^o_p}{R_p}\right]\right) \quad (9)$$

https://doi.org/10.1021/acsomega.2c01629
ACS Omega 2022, 7, 23380−23392

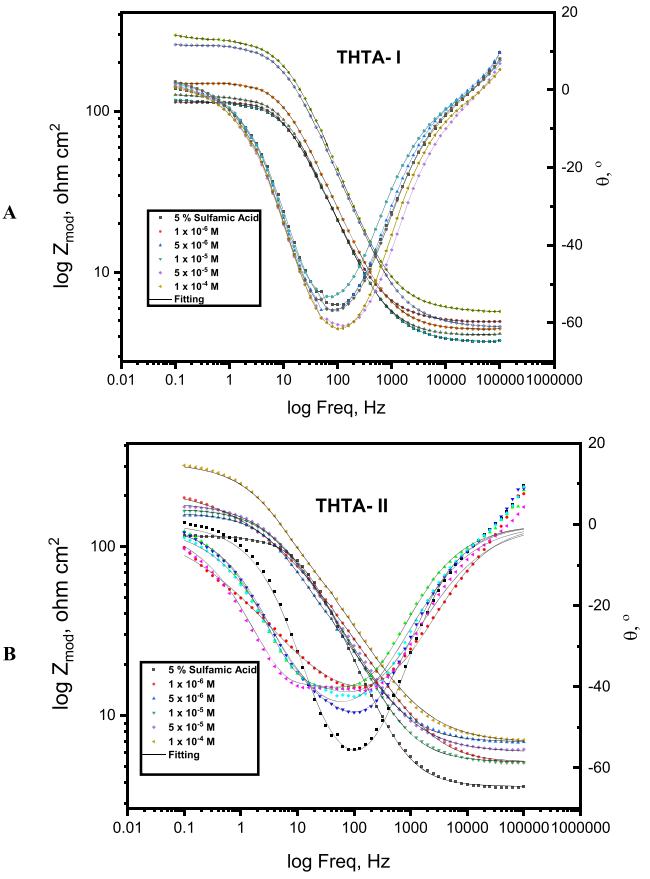

Figure 4. Bode diagrams for the corrosion of N80 carbon steel in 5% sulfamic acid medium involving different doses of **THTA** components (A) **THTA-I**, and (B) **THTA-II** at 25 ± 1 °C.

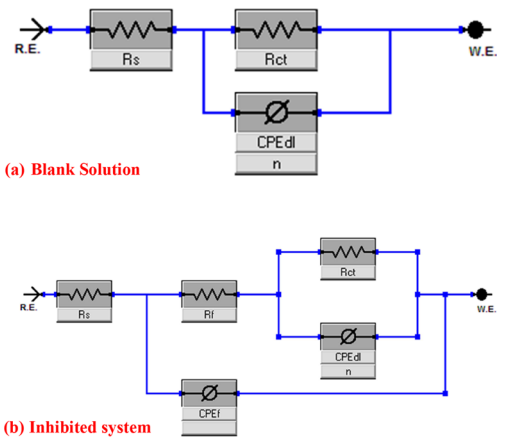

Figure 5. Equivalent circuit employed to fit the data obtained from EIS technique (a) using a blank solution, and (b) with different portions of the examined inhibitors.

The polarization resistances of N80 samples in 5% sulfamic acid media with and free **THTA** components are R_p^o and R_p, respectively.

The impedance Z_{CPE} can be considered using the formula:[47,48]

$$Z_{CPE} = \frac{1}{Y_0(j\omega)^n} \quad (10)$$

wherein Y_0 is the CPE admission, j is the imagined digit, ω is the angular frequency ($\omega = 2\pi f$), and n is the CPE index determined as a phase shift. Whenever $n = 0$, CPE designates a resistor; whenever $0 < n < 1$, it designates a not perfect capacitor; whenever $n = 1$, it represents a perfect capacitor.

The nonideal capacitive action is assigned to the heterogeneousness of metal specimens because of the unevenness of the N80 steel, dispersion of energetic positions, metal dissolution, contaminants, and the adsorption of the tested components on the N80 exterior, which is represented by the standards of the n index change within 0.451 to 0.994.

Table 3 lists the electrochemical variables discovered during EIS experiments. The higher R_{ct} standards of N80 steel in corrosive media containing 5% sulfamic acid contain **THTA** components, demonstrating that the inhibition efficiency of N80 steel specimens was demonstrated by **THTA** inhibitor adsorption on N80 steel specimens as well as the permutation of adsorbed water particles on the N80 surface.

The consequential reduction in the access of CPE standards was assigned to the **THTA** inhibitor adsorption on the N80 specimens, which expanded the width of the electrical double layer and inhibitor layer barrier based on **THTA** particle adsorption on the N80 surface. The investigations exhibited the corrosion inhibition capability of **THTA-I** > **THTA-II** at different concentrations of **THTA** components.

3.3. Surface Morphology by XPS Examinations. XPS tests were used to identify, discriminate, and confirm the chemical bonding and configuration of the **THTA-I** component and the adsorption mechanism of **THTA-I** particles on the N80 steel exterior. As shown in Figure 6, the XPS spectra were recorded for the N80 steel surface corroded in 5% sulfamic acid with the **THTA-I** compound. The peaks for C 1s, Fe 2p, O 1s N 1s, and S 2p were discovered in samples treated with the **THTA-I** compound, indicating the **THTA-I** molecule adsorption on the N80 exterior. The binding energies (Bes; eV) and corresponding appointments of each peak ingredient are recorded in Table 4.

The simple spectra of C 1s presented four peaks (Figure 6), with that at 285.41 eV assigned to the existence of −C−C−, −C═C−, and C−H bonds; that at 286.89 eV was credited to the presence of the −C−N bond; that at 287.55 eV was attributed to the C═N bond; and that at 288.95 eV was assigned to the C═N^+ bond.[49,50] The XPS spectra of Fe 2p for the treatment with the **THTA-I** compound demonstrated eight typical peaks (Figure 6), with 711.26 eV assigned to the Fe 2p3/2 of Fe^{2+}, 713.10 eV to the Fe 2p3/2 of Fe^{3+},[51] 719.01 eV to Fe 2p3/2 satellites of Fe^{2+}, 721.09 eV to Fe 2p3/2 satellites of Fe^{3+},[52] 724.36 eV to the Fe 2p1/2 of Fe0, 726.65 eV to the Fe 2p1/2 of Fe^{2+}, 729.65 eV to the Fe 2p1/2 of Fe^{3+}, and 734.49 eV to the Fe 2p1/2 satellites of Fe^{2+}.[53,54] Moreover, the high-resolution O 1s spectrum for the **THTA-I** compound revealed three peaks (Figure 6): the first (530.21 eV) was attributed to O^{2-} and may be associated with O^- atoms bonded to $Fe^{2+}$and Fe^{3+} in FeO and Fe_2O_3 oxides,[55,56] respectively; the second (531.70 eV) was attributed to OH^- that can be bonded to Fe^{3+} in FeO.OH and the third (532.25 eV) was assigned to the adsorbed water molecules.[57,58]

Moreover, the N80 steel in 5% sulfamic containing **THTA-I** exhibited N 1s spectra with three peaks (Figure 6) at 399.21 eV for sp^3 bonding (C−N), 400.17 eV for sp^2 bonding (C═N), and 401.07 eV for C═N^+, all of which are present in the **THTA-I** molecule.[59,60] Furthermore, the S 2p spectra included one characteristic peak (Figure 6) at 168.63 eV, and it was

https://doi.org/10.1021/acsomega.2c01629
ACS Omega 2022, 7, 23380−23392

Table 3. Electrochemical Kinetic Variables Acquired by EIS for N80 Carbon Steel in 5% Sulfamic Acid Media Including Diverse Doses of THTA at 25 ± 1 °C

concentration, M		R_s, Ω cm^2	$Y_{0,f} \times 10^{-6}$, s^n Ω^{-1} cm^{-2}	n_f	R_p, Ω cm^2	$Y_{0,dl}$ c10^{-6}, s^n Ω^{-1} cm^{-2}	n_{dl}	R_{ct}, Ω cm^2	θ	IE/%
5% sulfamic acid		3.77				233.2	0.827	28.8 ± 1.8		
THTA-I	1×10^{-6}	5.01	105.5	0.903	13.5	106.4	0.838	112.7 ± 7.9	74.5	74.5
	5×10^{-6}	4.16	52.57	0.978	7.4	167.6	0.790	113.40 ± 8.1	74.6	74.6
	1×10^{-5}	4.49	94.92	0.902	24.1	86.26	0.828	121.8 ± 8.8	76.4	76.4
	5×10^{-5}	4.69	65.28	0.880	13.7	47.37	0.770	240.6 ± 16.2	88.0	88.0
	1×10^{-4}	5.77	91.28	0.848	26.4	3.305	0.994	250.5 ± 17.4	88.5	88.5
THTA-II	1×10^{-6}	5.27	272	0.776	70.1	631.90	0.704	93.0 ± 6.5	0.691	69.1
	5×10^{-6}	6.94	395	0.731	66.2	371	0.834	96.9 ± 6.8	0.703	70.3
	1×10^{-5}	6.03	594	0.669	165.0	77.16	0.669	120.0 ± 8.6	0.760	76.0
	5×10^{-5}	6.86	498	0.641	177.7	193.20	0.986	131.6 ± 9.5	0.781	78.1
	1×10^{-4}	5.26	122	0.786	6.6	1328	0.451	215.0 ± 14.5	0.866	86.6

assigned to the $-SO_3^{2-}$ group exhibited in the sulfamic acid solution.[57] We confirmed the mechanism of **THTA-I** adsorption on the N80 surface in 5% sulfamic acid solution, which was in agreement with the XPS data.

3.4. DFT Computations. The interaction range in the active locations of triazine derivative components with the N80 steel surface was examined using DFT simulations. Furthermore, quantum chemical variables are designed in Table 5. Figure 7 displays the optimal constructs, highest occupied molecular orbital (HOMO), and lowest unoccupied molecular orbital (LUMO) for the examined inhibitors. HOMO and LUMO energies were allocated to the studied inhibitor's provider and receiver capabilities at the interface of inhibitor/metal exterior, in accordance with the FMO hypothesis.[61] Consequently, components with large E_{HOMO} and small E_{LUMO} values were considered to be better corrosion inhibitors.

Table 5 shows that the **THTA-I** compound had a larger E_{HOMO} value of −4.50 eV than the **THTA-II** molecule (−4.70 eV). The HOMO point was placed on the triazine, tetraazene, phenyl, and naphthalenol rings for the inhibitor compounds (Figure 7), indicating that N and O atoms were selected as sites for the electrophilic approach on the N80 steel exterior. Such arguments confirmed capability of the analyzed compounds to adsorb on N80's exterior and, consequently, increased the prohibition productivity along with experimental results. Furthermore, the E_{LUMO} values for **THTA-I** (Table 5) were −2.99 eV lower than for **THTA-II** (−2.46 eV), which is consistent with experimental results, and **THTA-I** had a higher inhibitory potency than **THTA-II**. Moreover, the energy difference (ΔE) is an important indicator of prohibition productivity, which increases as the ΔE value reduces.[62] Table 5 shows that **THTA-I** has a smaller ΔE value (1.52 eV) than **THTA-II** (2.24 eV) confirming that **THTA-I** has a greater tendency to be adsorbed on the N80 steel exterior. Furthermore, the low values of electronegativity (χ) provide a high potential reactivity for the examined inhibitors to allow electrons to the investigated surface; however, **THTA-I** has a greater value of χ (3.75) than **THTA-II** (3.58), signifying agreement with experimental conclusions; moreover, **THTA-I** has greater inhibition tendency than **THTA-II**.[63] Furthermore, the compound stability and susceptibility can be determined by hardness (η) and softness (σ), that is, soft compounds have additional protected potency than hard compounds owing to the smooth delivery of electrons to the N80 steel exterior during the adsorption, thus, they were evaluated as effective protective inhibitors.[64] As evidenced in Table 5, **THTA-I** has lower η values and greater σ values than **THTA-II**, indicating that **THTA-I** has a high potency for donating electrons to the examined steel and more prohibition potency.

The fraction of the charge transfer, ΔN values indicates how the compound possibly donates electrons to the steel sample; the higher the ΔN value, the more likely the compound is to donate.[65] As per the computed ΔN values in Table 5, **THTA-I** (0.70) has a higher ΔN value than **THTA-II** (0.55). Thus, **THTA-I** is more prone to deliver electrons to the N80 sample than **THTA-II**. Moreover, when $\eta > 0$ the $\Delta E_{back\text{-}donation}$ will be <0, indicating that an electron will then be transported to a compound afterward, a back-donation from the inhibitor and it will be better selected.[32] The calculated $\Delta E_{back\text{-}donation}$ standards for triazine compounds in Table 5 are negative (−0.19, −0.28), indicating that back-donation was favored for the investigated inhibitors that formed a strong connection with the steel samples.[66]

Furthermore, the dipole moment is a significant indicator for predicting inhibition efficiency.[67] The increase in dipole moment increased the deformation energy and chemical adsorption on the examined steel. Consequently, increasing the dipole moment increased the corrosion inhibition potency.[69,70] Table 5 shows that **THTA-I** has a higher dipole moment value (8.77 debye) than **THTA-II** (6.89 debye), indicating that **THTA-I** has a greater potency to be adsorbed on the tested N80 steel which improves the protection efficiency.

Furthermore, the propensity of the examined particles for preserving the N80 surface in corrosive media was linked to the molecular surface area. Given the contact region within the inhibitor compounds and the increased surface area of the N80 steel, the prohibition effectiveness boosted with the molecular surface area increments. As shown in Table 5, **THTA-I** demonstrated the greatest molecular surface area, which is supported by experimental evidence, whereas the highest prohibition potency was observed for **THTA-I** (696.15 $\AA^2$) than **THTA-II** (454.51 $\AA^2$).

Furthermore, using the Dmol^3 module, MEP mapping may be employed to examine the higher energetic locations of **THTA** inhibitors. The MEP mapping is a 3D visual descriptor that has been proposed to identify the whole electrostatic effect of a molecule based on general charge dispensation.[68] The red-colored image in Figure 8 shows the highest electron density area in the MEP maps; the MEP is always more negative (nucleophilic reaction). The blue colors, however, denote the highest positive domains (electrophilic reaction).[70] The highest negative domains are typically above triazine and phenyl moieties, as per the optical analysis in Figure 8.

https://doi.org/10.1021/acsomega.2c01629
ACS Omega 2022, 7, 23380−23392

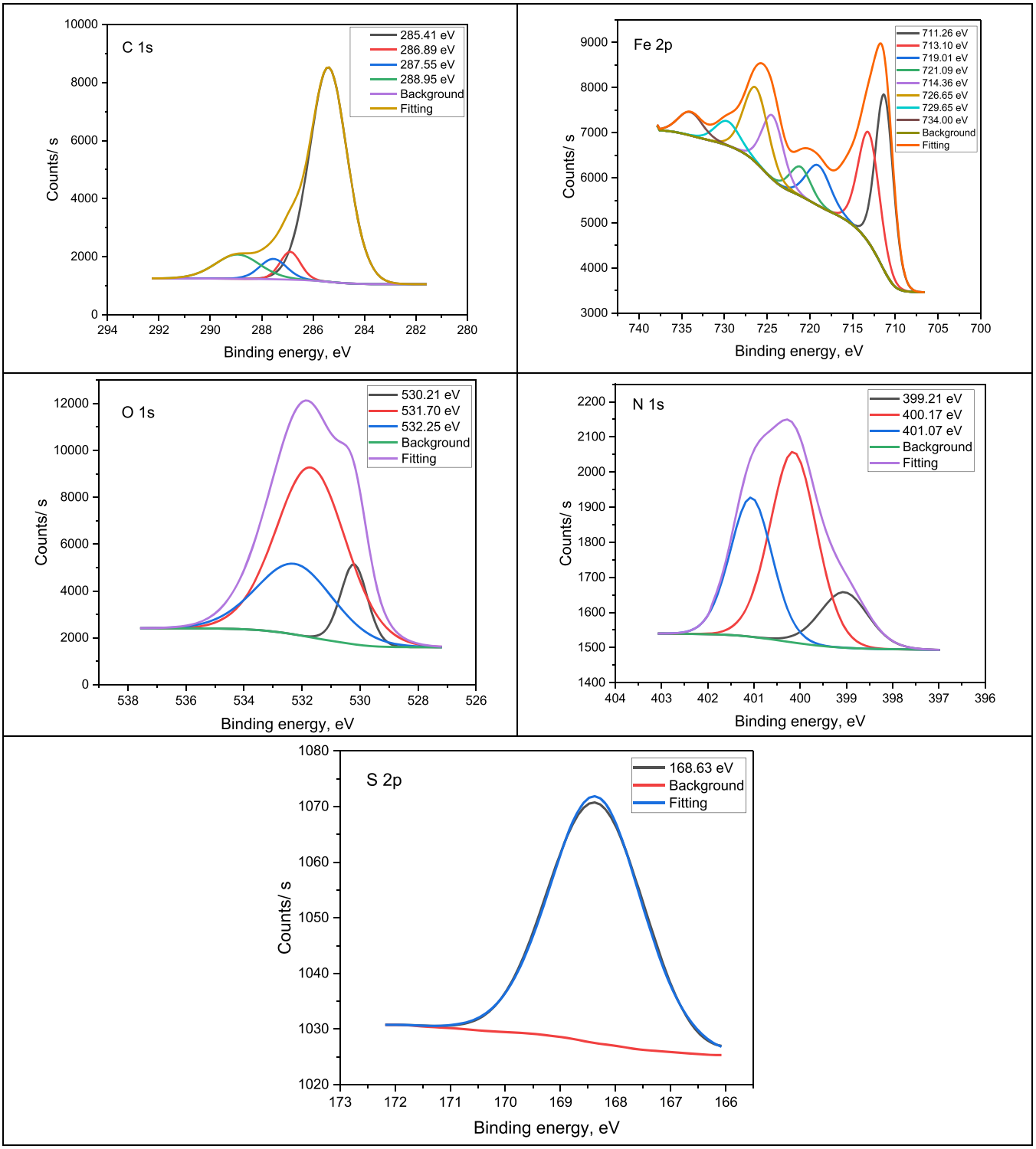

Figure 6. XPS plots of C 1s, Fe 2p, O 1s, N 1s, and S 2p for N80 carbon steel in 5% sulfamic acid solutions with 1×10^{-4} M of the **THTA-I** compound.

However, the electron density over the tetraazene moieties in the studied components was lower. For **THTA** compounds, MEP mapping demonstrated the most available positive locations over hydrogen atoms. The positions with high electron density (i.e., red areas) in the tested inhibitors may be most suited for correlations inside the steel, thus yielding a firmly adsorbed protecting film.

3.5. MC Simulations. The MC simulations aimed to indicate any evident adsorption mechanism and distinguish the correlations between the examined particles and steel specimens. Figure 9 shows the most acceptable adsorption formation, which is virtually flat, for the **THTA** particles on the N80 steel specimens, indicating an increase in adsorption locator and maximum surface covering.[71] Table 6 shows the obtained values for the adsorption energies derived from MC

https://doi.org/10.1021/acsomega.2c01629
ACS Omega 2022, 7, 23380−23392

Table 4. Binding Energy (eV) and Their Assignments for the Best Core Lines Noted for the N80 Carbon Steel Surface in 5% Sulfamic Processed with THTA-I Inhibitor

5% sulfamic acid treated with 1×10^{-4} M **THTA-I** inhibitor		
core element	BE, eV	assignments
C 1s	285.41	−C−H, −C−C−, −C═C−
	286.89	−C−N
	287.55	−C═N
	288.95	$-C{=}N^{+}$
Fe 2p	711.26	Fe $2p_{3/2}$ of Fe^{2+} in FeO $FeCl_2$
	713.10	Fe $2p_{3/2}$ of Fe^{3+} in Fe_2O_3, Fe_3O_4, FeOOH
	719.01	satellite Fe $2p_{3/2}$ of Fe^{2+} in FeO
	721.09	satellite Fe $2p_{3/2}$ of Fe^{3+} in Fe_2O_3, Fe_3O_4
	724.36	Fe $2p_{1/2}$ of Fe^{0} in FeO
	726.65	Fe $2p_{1/2}$ of Fe^{2+} in FeO
	729.65	Fe $2p_{1/2}$ of Fe^{3+} in Fe_2O_3
	734.00	satellite Fe $2p_{1/2}$ of Fe^{2+} in Fe_2O_3, Fe_3O_4
O 1 s	530.21	FeO, Fe_2O_3
	531.70	FeOOH
	532.25	adsorbed water molecules
N 1s	399.21	sp^3 bonding (C−N)
	400.17	sp^2 bonding (C═N)
	401.07	$C{=}N^{+}$
S 2p	168.63	$-SO_3^{2-}$

Table 5. Intended Quantum Chemical Variables for THTA Derivatives

inhibitor	THTA-I	THTA-II
E_{HOMO}, eV	−4.50	−4.70
E_{LUMO}, eV	−2.99	−2.46
ΔE, eV	1.52	2.24
I	4.50	4.70
A	2.99	2.46
X	3.75	3.58
H	0.76	1.12
Σ	1.32	0.89
ΔN	0.70	0.55
$\Delta E_{back\text{-}donation}$, eV	−0.19	−0.28
dipole moment value, debye	8.77	6.89
molecular surface area, Å^2	696.15	454.51

simulations. **THTA-I** (−2696.48 kcal mol^{-1}) has a larger negative value of the adsorption energy than **THTA-II** (−2671.58 kcal mol^{-1}), indicating that **THTA-I** has a strong adsorption on the N80 surface; moreover, it forms a strongly adsorbed barrier that inhibits the corrosion of N80 steel. These obtained data support the experimental results.[72] Table 6 demonstrates that the adsorption energies for **THTA-I** in the pregeometry optimization stage, that is, unrelaxed (−2845.38 kcal mol^{-1}) are higher negative than **THTA-II** (−2803.64 kcal mol^{-1}) and in the postgeometry optimization stage, that is, relaxed (148.90 kcal mol^{-1}) is greater than that of **THTA-I** (132.06 kcal mol^{-1}), declaring a greater prohibition potency for **THTA-I** compared with **THTA-II**.

If the adsorbed investigated compounds or water molecule is ignored, the dE_{ads}/dN_i values can be used to explain the metal-adsorbate structure energy.[73] Table 6 shows that the dE_{ads}/dN_i values for **THTA-I** (−190.31 kcal mol^{-1}) is higher than that for **THTA-II** (−173.09 kcal mol^{-1}), indicating that **THTA-I** has a better adsorption than **THTA-II**. Furthermore, the water (dE_{ads}/dN_i) values were close (−13.91 kcal mol^{-1}) to the

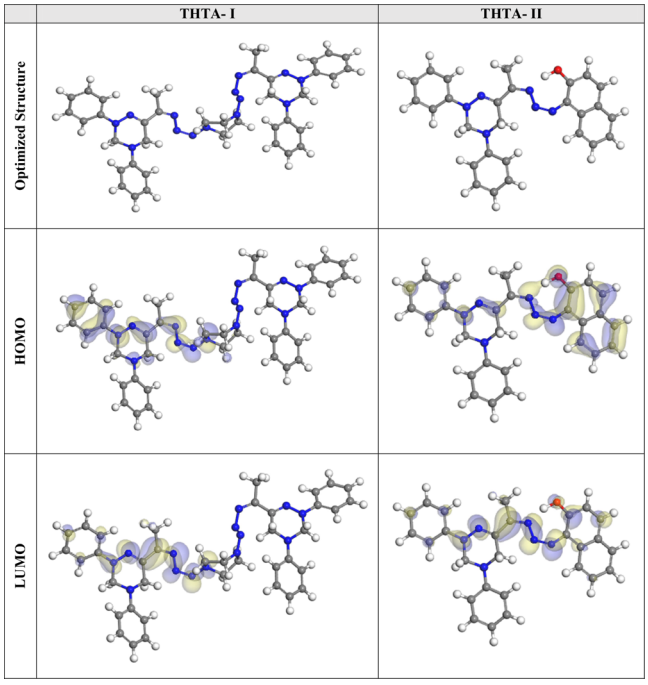

Figure 7. Optimized molecular configuration, HOMO and LUMO of the **THTA** inhibitors via the DMol3 module

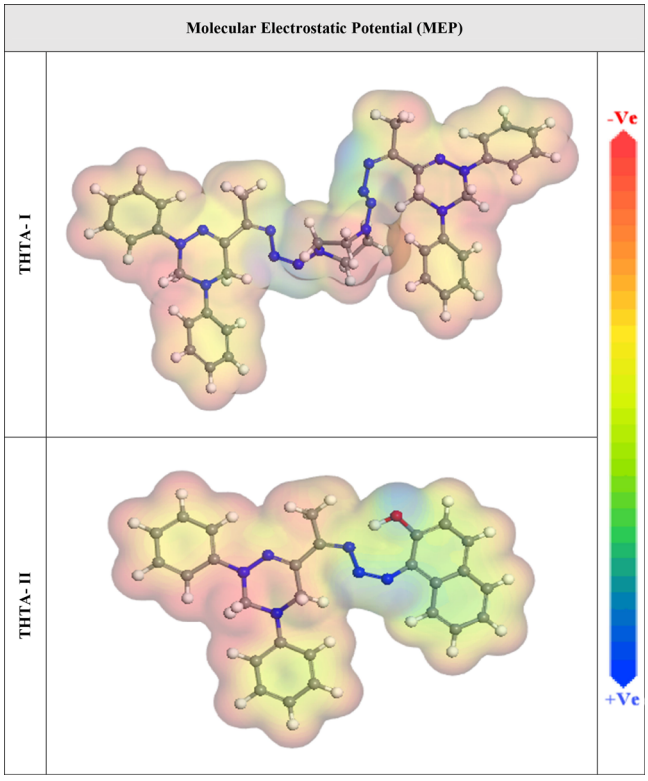

Figure 8. Visual diagram for MEP of the **THTA** inhibitors via the DMol^3 module.

triazine derivative values, indicating that the examined particles have strong adsorption relative to the 250 water molecules used, which helps in the swapping of water molecules by **THTA** compounds. Hence, the investigated compounds were powerfully adsorbed on steel samples, thus providing a strongly adsorbed preventive barrier that offered a steel sample

https://doi.org/10.1021/acsomega.2c01629
ACS Omega 2022, 7, 23380−23392

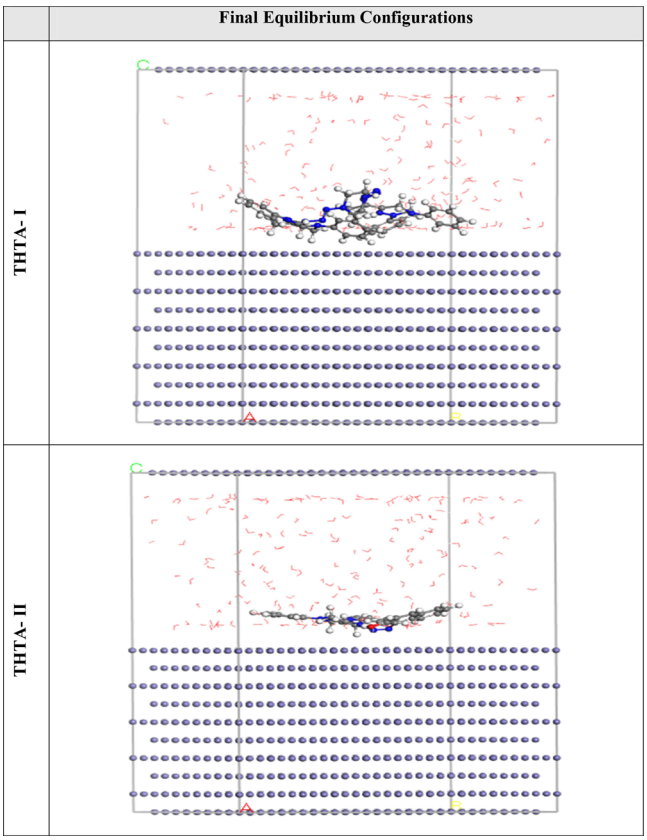

Figure 9. Best appropriate configurations for the adsorption of **THTA** inhibitors on Fe (1 1 0) substrate acquired by the adsorption locator module.

prohibition in 5% sulfamic acid medium, as determined by experimental and computational examinations.

3.6. Inhibition Mechanism of THTA Components. The results of different electrochemical techniques revealed that **THTA** compounds protected the tested N80 carbon steel surface from corrosion in 5% sulfamic acid solutions. The **THTA** inhibitors' prohibitive effectiveness can be related to the examined components' adsorption on the evaluated steel surface, which reduced the exposed surface area to the corrosive medium.

THTA inhibitors have more active sites for π-electrons as aromatic phenyl moieties and several heteroatoms, such as O and N; therefore, the adsorption of the investigated **THTA** inhibitors increased in the sequence of **THTA-I** > **THTA-II**.[74] **THTA** inhibitors existed in the protonated form in the sulfamic acid medium.[74] In sulfamic acid solutions, N80 specimens are positively charged.[75] Hence, the adsorption process can occur via $-SO_3NO_2^-$ anions, which are initially adsorbed onto the protonated N80 surface, to yield a negatively charged film. Therefore, the adsorption of the protonated form of **THTA** components will be restrained by the anion's concentration on the N80 surface. **THTA** compounds are likewise adsorbed by donor−acceptor correlations within the undivided electron pairs of (**N** and **O**) heteroatoms and π-electron of each (C═C) to create a coordinate bond through the vacant *d*-orbitals of Fe atoms on the N80 metal, which acts as a Lewis's acid and the development of a preventive chemisorbed barrier.[76−78] This result was confirmed with ΔG^0_{ads} values, which were greater than −40 kJ/mol confirming the chemisorption adsorption of

Table 6. Statistics and Descriptions Intended by the MC Simulation for the Adsorption of the Investigated Inhibitors on the Fe (1 1 0) Surface

structures	adsorption energy/kcal mol^{-1}	rigid adsorption energy/kcal mol^{-1}	deformation energy/kcal mol^{-1}	dE_{ads}/dN_i: inhibitor kcal mol^{-1}	dE_{ads}/dN_i: water kcal mol^{-1}
Fe (110)	−2696.48	−2845.38	148.90		
THTA-I				−190.31	
water					−13.97
Fe (110)	−2671.58	−2803.64	132.06		
THTA-II				−173.09	
water					−13.84

https://doi.org/10.1021/acsomega.2c01629
ACS Omega 2022, 7, 23380−23392

THTA compounds of N80 carbon steel in 5% sulfamic acid medium. The improved inhibition tendency of **THTA-I** was ascribed to the presence of an additional phenyl moiety, which has active spots that are prone to electrophilic attack and the smallest values for HOMO energy, ΔE, and hardness.[79]

4. CONCLUSIONS

- The tested inhibitors were efficient in inhibiting corrosion of N80 carbon steel metal in 5% sulfamic acid media, indicating that they were mixed-type inhibitors.
- The electrochemical data obtained from whole measurements confirmed that the inhibition potency improved with the concentrations increment. The %IE was accepted with the sequence of **THTA-I** > **THTA-II**.
- Double-layer capacitances diminished with reference to 5% sulfamic acid solution before the tested **THTA** inhibitors were added. Such a result may be confirmed by the adsorption mechanism of **THTA** compounds onto the N80 steel surface.
- The Langmuir adsorption isotherm was the appropriate isotherm for the adsorption of the tested **THTA** compounds on the N80 steel surface in 5% sulfamic acid solutions.
- The negative values of ΔG^0_{ads}demonstrated the spontaneity of the adsorption.
- XPS was performed to support the adsorption of **THTA-I** onto the N80 steel surface.
- The inhibition capacity values obtained from the whole electrochemical methods (PP and EIS) demonstrated the authenticity of the received data, and an upstanding agreement was observed within the experimental and theoretically obtained data.

AUTHOR INFORMATION

Corresponding Authors

Hany M. Abd El-Lateef − *Department of Chemistry, College of Science, King Faisal University, Al-Ahsa 31982, Saudi Arabia; Department of Chemistry, Faculty of Science, Sohag University, Sohag 82524, Egypt*; Email: hmahmed@kfu.edu.sa

Yasser M. Abdallah − *Dental Biomaterials Department, Faculty of Oral and Dental Medicine, Delta University for Science and Technology, Gamasa, Mansoura 11152, Egypt*; orcid.org/0000-0001-9116-5123; Email: dr.ymostafa8@gmail.com, yasser.mostafa@deltauniv.edu.eg

Authors

Kamal Shalabi − *Department of Chemistry, College of Science and Humanities in Al-Kharj, Prince Sattam bin Abdulaziz University, Al-Kharj 11942, Saudi Arabia; Chemistry Department, Faculty of Science, Mansoura University, Mansoura 35111, Egypt*; orcid.org/0000-0001-5478-6369

Anas M. Arab − *Chemistry Department, Faculty of Science, Mansoura University, Mansoura 35111, Egypt*

Complete contact information is available at: https://pubs.acs.org/10.1021/acsomega.2c01629

Author Contributions

H.M.A.E.-L.: Investigation, formal analysis, data curation, funding acquisition, writing-original draft, and writing-review and editing. K.S.: Investigation, supervision, methodology, resources, formal analysis, data curation, writing-original draft, and writing-review and editing. A.M.A.: Conceptualization, supervision, investigation, methodology, resources, formal analysis, data curation, writing-original draft, and writing-review and editing. Y.M.A.: Conceptualization, supervision, investigation, methodology, resources, formal analysis, data curation, writing-original draft, and writing-review and editing.

Notes

The authors declare no competing financial interest.

ACKNOWLEDGMENTS

This work was supported through the Annual Funding track by the Deanship of Scientific Research, Vice Presidency for Graduate Studies and Scientific Research, King Faisal University, Saudi Arabia [GRANT-536].

REFERENCES

(1) Touir, R.; Cenoui, M.; El Bakri, M.; Ebn Touhami, M. Sodium Gluconate as Corrosion and Scale Inhibitor of Ordinary Steel in Simulated Cooling Water. *Corros. Sci.* **2008**, *50*, 1530−1537.

(2) Li, X.; Deng, S.; Fu, H. Triazolyl Blue Tetrazolium Bromide as a Novel Corrosion Inhibitor for Steel in HCl and H_2SO_4 Solutions. *Corros. Sci.* **2011**, *53*, 302−309.

(3) Labriti, B.; Dkhireche, N.; Touir, R.; Ebn Touhami, M.; Sfaira, M.; El Hallaoui, A.; Hammouti, B.; Alami, A. Synergism in Mild Steel Corrosion and Scale Inhibition by a New Oxazoline in Synthetic Cooling Water. *Arab. J. Sci. Eng.* **2012**, *37*, 1293−1303.

(4) Javadian, S.; Yousefi, A.; Neshati, J. Synergistic Effect of Mixed Cationic and Anionic Surfactants on the Corrosion Inhibitor Behavior of Mild Steel in 3.5% NaCl. *Appl. Surf. Sci.* **2013**, *285*, 674−681.

(5) Zarrok, H.; Zarrouk, A.; Hammouti, B.; Salghi, R.; Jama, C.; Bentiss, F. Corrosion Control of Carbon Steel in Phosphoric Acid by Purpald-Weight Loss, Electrochemical and XPS Studies. *Corros. Sci.* **2012**, *64*, 243−252.

(6) Yassin, A. Y.; Abdelghany, A. M.; Shaban, M. M.; Abdallah, Y. M. Synthesis, Characterization and Electrochemical Behavior for API 5L X70 Carbon Steel in 5% Sulfamic Acid Medium Using PVVH/PEMA Blend Filled with Gold Nanoparticles. *Colloids Surf., A* **2022**, *635*, No. 128115.

(7) Raupach, M.; Elsener, B.; Polder, R.; Mietz, J. *Corrosion of Reinforcement in Concrete*; Woodhead Publishing Limited, 2007.

(8) Söylev, T. A.; Richardson, M. G. Corrosion Inhibitors for Steel in Concrete: State-of-the-Art Report. *Constr. Build. Mater.* **2008**, *22*, 609−622.

(9) Abdallah, Y. M.; Shalabi, K.; Bayoumy, N. M. Eco-Friendly Synthesis, Biological Activity and Evaluation of Some New Pyridopyrimidinone Derivatives as Corrosion Inhibitors for API 5L X52 Carbon Steel in 5% Sulfamic Acid Medium. *J. Mol. Struct.* **2018**, *1171*, 658−671.

(10) Hermas, A. A.; Morad, M. S. A Comparative Study on the Corrosion Behaviour of 304 Austenitic Stainless Steel in Sulfamic and Sulfuric Acid Solutions. *Corros. Sci.* **2008**, *50*, 2710−2717.

(11) El Azhar, M.; Mernari, B.; Traisnel, M.; Bentiss, F.; Lagrenée, M. Corrosion Inhibition of Mild Steel by the New Class of Inhibitors [2,5-Bis(n-Pyridyl)-1,3,4-Thiadiazoles] in Acidic Media. *Corros. Sci.* **2001**, *43*, 2229−2238.

(12) Shalabi, K.; Abdallah, Y. M.; Hassan, H. M.; Fouda, A. S. Adsorption and Corrosion Inhibition of Atropa Belladonna Extract on Carbon Steel in 1 M HCl Solution. *Int. J. Electrochem. Sci.* **2014**, *9*, 1468−1487.

(13) Abdel-Fatah, H. T. M.; Rashwan, S. A. M.; Abd El Wahaab, S. M.; Hassan, A. A. M. Effect of Tryptophan on the Corrosion Behavior of Low Alloy Steel in Sulfamic Acid. *Arab. J. Chem.* **2016**, *9*, S1069−S1076.

(14) Obaid, A. Y.; Ganash, A. A.; Qusti, A. H.; Elroby, S. A.; Hermas, A. A. Corrosion Inhibition of Type 430 Stainless Steel in an

Acidic Solution Using a Synthesized Tetra-Pyridinium Ring-Containing Compound. *Arab. J. Chem.* **2017**, *10*, S1276−S1283.
(15) Holze, R. Jacek Lipkowski and Philip N. Ross (Eds.): Adsorption of Molecules at Metal Electrodes, VCH Weinheim. New York 1992. ISBN 3-527-28008-1, 413 Seiten, Preis: DM 246. In *Berichte der Bunsengesellschaft für physikalische Chemie*; Wiley, 1993; Vol. *97*, pp 644−645, DOI: 10.1002/bbpc.19930970426.
(16) Abdel-Fatah, H. T. M.; Hassan, A. A. M.; Saadi, Z. A.; Shetify, M. M.; El-Sehiety, H. E. E. Corrosion Inhibition of Mild Steel in Acidic Medium by Salvadora Persica (Miswak) − Part 1: In Sulfamic Acid. *Chem. Sci. Trans.* **2014**, *3*, 221−231.
(17) Motamedi, M.; Tehrani-Bagha, A. R.; Mahdavian, M. A Comparative Study on the Electrochemical Behavior of Mild Steel in Sulfamic Acid Solution in the Presence of Monomeric and Gemini Surfactants. *Electrochim. Acta* **2011**, *58*, 488−496.
(18) Motamedi, M.; Tehrani-Bagha, A. R.; Mahdavian, M. Effect of Aging Time on Corrosion Inhibition of Cationic Surfactant on Mild Steel in Sulfamic Acid Cleaning Solution. *Corros. Sci.* **2013**, *70*, 46−54.
(19) Nechak, R.; Bouzroura, S. A.; Benmalek, Y.; Salhi, L.; Martini, S. P.; Morizur, V.; Dunach, E.; Kolli, B. N. Synthesis and Antimicrobial Activity Evaluation of Novel 4-Thiazolidinones Containing a Pyrone Moiety. *Synth. Commun.* **2014**, *45*, 262−272.
(20) Ramagiri, R. K.; Vedula, R. R.; Thupurani, M. K. A. Facile One-Step Multi-Component Approach toward the Synthesis of 3-(2-Amino-4-Thiazolyl) Coumarins by Using Trimethylsilyl Isothiocyanate and Their Antioxidant and Anti-Inflammatory Activity. *Phosphorus, Sulfur Silicon Relat. Elem.* **2015**, *190*, 1393−1397.
(21) Branowska, D.; Farahat, A. A.; Kumar, A.; Wenzler, T.; Brun, R.; Liu, Y.; Wilson, W. D.; Boykin, D. W. Synthesis and Antiprotozoal Activity of 2,5-Bis[Amidinoaryl]Thiazoles. *Bioorg. Med. Chem.* **2010**, *18*, 3551−3558.
(22) Makam, P.; Thakur, P. K.; Kannan, T. In Vitro and in Silico Antimalarial Activity of 2-(2-Hydrazinyl)Thiazole Derivatives. *Eur. J. Pharm. Sci.* **2014**, *52*, 138−145.
(23) Dawood, K. M.; Eldebss, T. M. A.; El-Zahabi, H. S. A.; Yousef, M. H.; Metz, P. Synthesis of Some New Pyrazole-Based 1,3-Thiazoles and 1,3,4-Thiadiazoles as Anticancer Agents. *Eur. J. Med. Chem.* **2013**, *70*, 740−749.
(24) Ravichandran, V.; Prashantha Kumar, B. R.; Sankar, S.; Agrawal, R. K. Predicting Anti-HIV Activity of 1,3,4-Thiazolidinone Derivatives: 3D-QSAR Approach. *Eur. J. Med. Chem.* **2009**, *44*, 1180−1187.
(25) Jagdish, K. S.; Swastika, G.; Atul, K. R. A Valuable Insight into Recent Developments and Biological Activities. *Chin. J. Nat. Med.* **2014**, *11*, 456−465.
(26) Afsah, E. M.; Arab, A. M.; Abdel-Galil, E. Synthesis and Biological Evaluation of Novel Tetrahydro-1,2,4-triazines Incorporating Triazene and Tetraazene Moieties. *ChemistrySelect* **2019**, *4*, 10649−10652.
(27) Abdel-Rehim, S. S.; Khaled, K. F.; Abd-Elshafi, N. S. Electrochemical Frequency Modulation as a New Technique for Monitoring Corrosion Inhibition of Iron in Acid Media by New Thiourea Derivative. *Electrochim. Acta* **2006**, *51*, 3269−3277.
(28) Parr, R. G.; Donnelly, R. A.; Levy, M.; Palke, W. E. Electronegativity: The Density Functional Viewpoint. *J. Chem. Phys.* **1978**, *68*, 3801−3807.
(29) Stern, M. Closure to "Discussion of 'Electrochemical Polarization, 1. A Theoretical Analysis of the Shape of Polarization Curves' [M. Stern and A. L. Geary (Pp. 56−63, Vol. 104)].". *J. Electrochem. Soc.* **1957**, *104*, 751−758.
(30) Abd El-Lateef, H. M. A.; Sayed, A. R.; Shalabi, K. Synthesis and Theoretical Studies of Novel Conjugated Polyazomethines and Their Application as Efficient Inhibitors for C1018 Steel Pickling Corrosion Behavior. *Surf. Interfaces* **2021**, *23*, No. 101037.
(31) Abd El-Lateef, H. M.; Shalabi, K.; Abdelhamid, A. A. One-Pot Synthesis of Novel Triphenyl Hexyl Imidazole Derivatives Catalyzed by Ionic Liquid for Acid Corrosion Inhibition of C1018 Steel: Experimental and Computational Perspectives. *J. Mol. Liq.* **2021**, *334*, No. 116081.
(32) Verma, D. K.; Aslam, R.; Aslam, J.; Quraishi, M. A.; Ebenso, E. E.; Verma, C. Computational Modeling: Theoretical Predictive Tools for Designing of Potential Organic Corrosion Inhibitors. *J. Mol. Struct.* **2021**, *1236*, No. 130294.
(33) Abdallah, Y. M.; Elzanaty, H. Electrochemical Studies on the Inhibition Behavior of Composite Udimet 700 − Alumina in 1 M Hydrochloric Acid by Some New Organic Derivatives. *Mater. Chem. Phys.* **2019**, *238*, No. 121925.
(34) Umoren, S. A.; Ekanem, U. F. Inhibition of Mild Steel Corrosion in H_2SO_4 Using Exudate Gum Frompachylobus Edulisand Synergistic Potassium Halide Additives. *Chem. Eng. Commun.* **2010**, *197*, 1339−1356.
(35) Bentiss, F.; Lebrini, M.; Vezin, H.; Chai, F.; Traisnel, M.; Lagrené, M. Enhanced Corrosion Resistance of Carbon Steel in Normal Sulfuric Acid Medium by Some Macrocyclic Polyether Compounds Containing a 1,3,4-Thiadiazole Moiety: AC Impedance and Computational Studies. *Corros. Sci.* **2009**, *51*, 2165−2173.
(36) Singh, D. K.; Kumar, S.; Udayabhanu, G.; John, R. P. 4(NN-Dimethylamino) Benzaldehyde Nicotinic Hydrazone as Corrosion Inhibitor for Mild Steel in 1 M HCl Solution: An Experimental and Theoretical Study. *J. Mol. Liq.* **2016**, *216*, 738−746.
(37) Hosseini, M.; Mertens, S. F. L.; Ghorbani, M.; Arshadi, M. R. Asymmetrical Schiff Bases as Inhibitors of Mild Steel Corrosion in Sulphuric Acid Media. *Mater. Chem. Phys.* **2003**, *78*, 800−808.
(38) Damaskin, B. B.; Petrii, O. A.; Batrakov, V. V. *Adsorption of Organic Compounds on Electrodes*; Springer US, 1971.
(39) Cohen, M. Sodium Hexametaphosphate as a Corrosion Inhibitor for Ottawa Tap Water. *Trans. Electrochem. Soc.* **1946**, *89*, 105.
(40) Khamis, E.; Bellucci, F.; Latanision, R. M.; El-Ashry, E. S. H. Acid Corrosion Inhibition of Nickel by 2-(Triphenosphoranylidene) Succinic Anhydride. *Corrosion* **1991**, *47*, 677−686.
(41) Barcia, O. E.; Mattos, O. R.; Pebere, N.; Tribollet, B. Mass-Transport Study for the Electrodissolution of Copper in 1M Hydrochloric Acid Solution by Impedance. *J. Electrochem. Soc.* **1993**, *140*, 2825−2832.
(42) Jüttner, K. Electrochemical Impedance Spectroscopy (EIS) of Corrosion Processes on Inhomogeneous Surfaces. *Electrochim. Acta* **1990**, *35*, 1501−1508.
(43) López, D. A.; Simison, S. N.; de Sánchez, S. R. Inhibitors Performance in CO_2 Corrosion. *Corros. Sci.* **2005**, *47*, 735−755.
(44) Khaled, K. F.; Hackerman, N. Investigation of the Inhibitive Effect of Ortho-Substituted Anilines on Corrosion of Iron in 1 M HCl Solutions. *Electrochim. Acta* **2003**, *48*, 2715−2723.
(45) Bentiss, F.; Jama, C.; Mernari, B.; El Attari, H.; El Kadi, L.; Lebrini, M.; Traisnel, M.; Lagrenée, M. Corrosion Control of Mild Steel Using 3,5-Bis (4-Methoxyphenyl)-4-Amino-1,2,4-Triazole in Normal Hydrochloric Acid Medium. *Corros. Sci.* **2009**, *51*, 1628−1635.
(46) Zheltikov, A. Impedance Spectroscopy: Theory, Experiment, and Applications Second Edition. Evgenij Barsoukov and J. Ross Macdonald (Eds). John Wiley & Sons, Inc., Hoboken, New Jersey, 2005, Pp. 595. *J. Raman Spectrosc* **2006**, *38*, 122.
(47) Rosalbino, F.; Scavino, G.; Mortarino, G.; Angelini, E.; Lunazzi, G. EIS Study on the Corrosion Performance of a Cr(III)-Based Conversion Coating on Zinc Galvanized Steel for the Automotive Industry. *J. Solid State Electrochem.* **2010**, *15*, 703−709.
(48) Raviprabha, K.; Bhat, R. S. Electrochemical and Quantum Chemical Studies of 5-[(4-Chlorophenoxy) Methyl]-4H-1,2,4-Triazole-3-Thiol on the Corrosion Inhibition of 6061 Al Alloy in Hydrochloric Acid. *J. Fail. Anal. Prev.* **2020**, *20*, 1598−1608.
(49) Ouici, H.; Tourabi, M.; Benali, O.; Selles, C.; Jama, C.; Zarrouk, A.; Bentiss, F. Adsorption and Corrosion Inhibition Properties of 5-Amino 1,3,4-Thiadiazole-2-Thiol on the Mild Steel in Hydrochloric Acid Medium: Thermodynamic, Surface and Electrochemical Studies. *J. Electroanal. Chem.* **2017**, *803*, 125−134.

https://doi.org/10.1021/acsomega.2c01629
ACS Omega 2022, 7, 23380−23392

(50) Fan, G.; Liu, H.; Fan, B.; Ma, Y.; Hao, H.; Yang, B. Trazodone as an Efficient Corrosion Inhibitor for Carbon Steel in Acidic and Neutral Chloride-Containing Media: Facile Synthesis, Experimental and Theoretical Evaluations. *J. Mol. Liq.* **2020**, *311*, No. 113302.
(51) Bouanis, M.; Tourabi, M.; Nyassi, A.; Zarrouk, A.; Jama, C.; Bentiss, F. Corrosion Inhibition Performance of 2,5-Bis (4-Dimethylaminophenyl)-1,3,4-Oxadiazole for Carbon Steel in HCl Solution: Gravimetric, Electrochemical and XPS Studies. *Appl. Surf. Sci.* **2016**, *389*, 952−966.
(52) Solomon, M. M.; Umoren, S. A.; Quraishi, M. A.; Salman, M. Myristic Acid Based Imidazoline Derivative as Effective Corrosion Inhibitor for Steel in 15% HCl Medium. *J. Colloid Interface Sci.* **2019**, *551*, 47−60.
(53) Hashim, N. Z. N.; Anouar, E. H.; Kassim, K.; Zaki, H. M.; Alharthi, A. I.; Embong, Z. XPS and DFT Investigations of Corrosion Inhibition of Substituted Benzylidene Schiff Bases on Mild Steel in Hydrochloric Acid. *Appl. Surf. Sci.* **2019**, *476*, 861−877.
(54) Bommersbach, P.; Alemany-Dumont, C.; Millet, J. P.; Normand, B. Formation and Behaviour Study of an Environment-Friendly Corrosion Inhibitor by Electrochemical Methods. *Electrochim. Acta* **2005**, *51*, 1076−1084.
(55) Temesghen, W.; Sherwood, P. Analytical Utility of Valence Band X-Ray Photoelectron Spectroscopy of Iron and Its Oxides, with Spectral Interpretation by Cluster and Band Structure Calculations. *Anal. Bioanal. Chem.* **2002**, *373*, 601−608.
(56) Zarrouk, A.; Hammouti, B.; Lakhlifi, T.; Traisnel, M.; Vezin, H.; Bentiss, F. New 1H-Pyrrole-2,5-Dione Derivatives as Efficient Organic Inhibitors of Carbon Steel Corrosion in Hydrochloric Acid Medium: Electrochemical XPS and DFT Studies. *Corros. Sci.* **2015**, *90*, 572−584.
(57) Mourya, P.; Singh, P.; Rastogi, R. B.; Singh, M. M. Inhibition of Mild Steel Corrosion by 1,4,6-Trimethyl-2-Oxo-1,2-Dihydropyridine-3-Carbonitrile and Synergistic Effect of Halide Ion in 0.5 M H_2SO_4. *Appl. Surf. Sci.* **2016**, *380*, 141−150.
(58) Kharbach, Y.; Qachchachi, F. Z.; Haoudi, A.; Tourabi, M.; Zarrouk, A.; Jama, C.; Olasunkanmi, L. O.; Ebenso, E. E.; Bentiss, F. Anticorrosion Performance of Three Newly Synthesized Isatin Derivatives on Carbon Steel in Hydrochloric Acid Pickling Environment: Electrochemical, Surface and Theoretical Studies. *J. Mol. Liq.* **2017**, *246*, 302−316.
(59) Zhao, M.; Cao, Y.; Liu, X.; Deng, J.; Li, D.; Gu, H. Effect of Nitrogen Atomic Percentage on N^+-Bombarded MWCNTs in Cytocompatibility and Hemocompatibility. *Nanoscale Res. Lett.* **2014**, *9*, 142.
(60) Harris, T. G. A. A.; Götz, R.; Wrzolek, P.; Davis, V.; Knapp, C. E.; Ly, K.; Hildebrandt, P.; Schwalbe, M.; Weidinger, I.; Zebger, I.; Fischer, A. Robust Electrografted Interfaces on Metal Oxides for Electrocatalysis − an in Situ Spectroelectrochemical Study. *J. Mater. Chem. A* **2018**, *6*, 15200−15212.
(61) Boulhaoua, M.; El Hafi, M.; Zehra, S.; Eddaif, L.; Alrashdi, A.; Lahmidi, S.; Guo, L.; Mague, J. T. J. T.; Lgaz, H. Synthesis, Structural Analysis and Corrosion Inhibition Application of a New Indazole Derivative on Mild Steel Surface in Acidic Media Complemented with DFT and MD Studies. *Colloids Surf., A* **2021**, *617*, No. 126373.
(62) Abd El-Lateef, H. M.; Shalabi, K.; Tantawy, A. H. Corrosion Inhibition and Adsorption Features of Novel Bioactive Cationic Surfactants Bearing Benzenesulphonamide on C1018-Steel under Sweet Conditions: Combined Modeling and Experimental Approaches. *J. Mol. Liq.* **2020**, *320*, No. 114564.
(63) Raviprabha, K.; Bhat, R. S. 5-(3-Pryridyl)-4H-1,2,4-Triazole-3-Thiol as Potential Corrosion Inhibitor for AA6061 Aluminium Alloy in 0.1 M Hydrochloric Acid Solution. *Surf. Eng. Appl. Electrochem.* **2019**, *55*, 723−733.
(64) Raviprabha, K.; Bhat, R. S. Inhibition Effects of Ethyl-2-Amino-4-Methyl-1,3-Thiazole-5-Carboxylate on the Corrosion of AA6061 Alloy in Hydrochloric Acid Media. *J. Fail. Anal. Prev.* **2019**, *19*, 1464−1474.
(65) Raviprabha, K.; Bhat, R. S. Corrosion Inhibition Effect of Ethyl 1-(4-Chlorophenyl)-5-Methyl-1H-1,2,3-Triazole-4-Carboxylate on Aluminium Alloy in Hydrochloric Acid. *Prot. Met. Phys. Chem. Surf.* **2021**, *57*, 181−189.
(66) Upadhyay, A.; Purohit, A. K.; Mahakur, G.; Dash, S.; Kar, P. K.; Kumar, A.; Mahakur, G.; Dash, S.; Kumar, P. Verification of Corrosion Inhibition of Mild Steel by Some 4-Aminoantipyrine-Based Schiff Bases−Impact of Adsorbate Substituent and Cross-Conjugation. *J. Mol. Liq.* **2021**, *333*, No. 115960.
(67) Abd El-Lateef, H. M.; Shalabi, K.; Tantawy, A. H. Corrosion Inhibition of Carbon Steel in Hydrochloric Acid Solution Using Newly Synthesized Urea-Based Cationic Fluorosurfactants: Experimental and Computational Investigations. *New J. Chem.* **2020**, *44*, 17791−17814.
(68) Oyebamiji, A. K.; Adeleke, B. B. Quantum Chemical Studies on Inhibition Activities of 2,3-Dihydroxypropyl-Sulfanyl Derivative on Carbon Steel in Acidic Media. *Int. J. Corros. Scale Inhib.* **2018**, *7*, 498−508.
(69) Madkour, L. H.; Kaya, S.; Obot, I. B. Computational, Monte Carlo Simulation and Experimental Studies of Some Arylazotriazoles (AATR) and Their Copper Complexes in Corrosion Inhibition Process. *J. Mol. Liq.* **2018**, *260*, 351−374.
(70) Hasanov, R.; Bilge, S.; Bilgiç, S.; Gece, G.; Kiliç, Z.; Kılıç, Z. Experimental and Theoretical Calculations on Corrosion Inhibition of Steel in 1M H_2SO_4 by Crown Type Polyethers. *Corros. Sci.* **2010**, *52*, 984−990.
(71) Shalabi, K.; Helmy, A. M. M.; El-Askalany, A. H.; Shahba, M. M. New Pyridinium Bromide Mono-Cationic Surfactant as Corrosion Inhibitor for Carbon Steel during Chemical Cleaning: Experimental and Theoretical Studies. *J. Mol. Liq.* **2019**, *293*, No. 111480.
(72) El Aadad, H.; Galai, M.; Ouakki, M.; Elgendy, A.; Touhami, M. E.; Chahine, A. Improvement of the Corrosion Resistance of Mild Steel in Sulfuric Acid by New Organic-Inorganic Hybrids of Benzimidazole-Pyrophosphate: Facile Synthesis, Characterization, Experimental and Theoretical Calculations (DFT and MC). *Surf. Interfaces* **2021**, *24*, No. 101084.
(73) Dehghani, A.; Mostafatabar, A. H.; Bahlakeh, G.; Ramezanzadeh, B. A Detailed Study on the Synergistic Corrosion Inhibition Impact of the Quercetin Molecules and Trivalent Europium Salt on Mild Steel; Electrochemical/Surface Studies, DFT Modeling, and MC/MD Computer Simulation. *J. Mol. Liq.* **2020**, No. 113914.
(74) Abdallah, M.; Megahed, H. E. Cyclic Voltammograms of Iron and C-Steels in Oxalic Acid Solutions and Investigation of the Effect of Phenyl Phthalimide as Corrosion Inhibitors. *Monatsh. Chem.* **1995**, *126*, 519−527.
(75) Solmaz, R.; Kardaş, G.; Yazıcı, B.; Erbil, M. Adsorption and Corrosion Inhibitive Properties of 2-Amino-5-Mercapto-1,3,4-Thiadiazole on Mild Steel in Hydrochloric Acid Media. *Colloids Surfaces A Physicochem. Eng. Asp.* **2008**, *312*, 7−17.
(76) Blomgren, E.; Bockris, J. O. M. The Adsorption of Aromatic Amines at the Interface: Mercury-Aqueous Acid Solution. *J. Phys. Chem.* **1959**, *63*, 1475−1484.
(77) Ahamad, I.; Quraishi, M. A. Mebendazole: New and Efficient Corrosion Inhibitor for Mild Steel in Acid Medium. *Corros. Sci.* **2010**, *52*, 651−656.
(78) Shalabi, K.; Abdel-Galil, E.; El-Askalany, A. H.; Abdallah, Y. M. Adsorption, Electrochemical Behavior, and Theoretical Studies for Copper Corrosion Inhibition in 1 M Nitric Acid Medium Using Triazine Derivatives. *J. Mol. Liq.* **2022**, *348*, No. 118420.
(79) Kumar, D.; Jain, N.; Jain, V.; Rai, B. Amino Acids as Copper Corrosion Inhibitors: A Density Functional Theory Approach. *Appl. Surf. Sci.* **2020**, *514*, No. 145905.

https://doi.org/10.1021/acsomega.2c01629
ACS Omega 2022, 7, 23380−23392